Acta Crystallographica Section A
Foundations of Crystallography
ISSN 0108-7673

Received 2 February 2004
Accepted 24 June 2004

Variable-temperature X-ray crystallographic studies: a complementary tool for charge-density investigation of soft (organometallic) bonds

Piero Macchi[a,b]* and Angelo Sironi[a,b]*

[a]Dipartimento di Chimica Strutturale e Stereochimica Inorganica, Università di Milano, via Venezian 21, 20133 Milano, Italy, and [b]Centro CNR, ISTM, Milano, Italy. Correspondence e-mail: piero.macchi@istm.cnr.it, angelo.sironi@istm.cnr.it

Comparative X-ray diffraction studies at different temperatures are used to complement the information usually extracted from 'single-point' charge-density studies. The response of soft bonds against (temperature driven) changes of the crystalline environment might be indicative of some intramolecular mode associated with an incipient bonding. This is in fact confirmed for the anion $[FeCo(CO)_8]^-$ in the $[(Ph_3P)_2N]^+$ salt. In contrast, the $[Cr_2H(CO)_{10}]^-$ anion, whose conformation is known to strongly depend on the counterion, is actually insensitive to T variations in the $[K(C_{18}H_{36}N_2O_6)]^+$ salt.

1. Introduction

As is well known, low temperature is necessary to measure accurate diffraction intensities and refine models to reconstruct the static electron density. In a seminal review article, Larsen (1995) illustrated the additional advantages of using temperatures below the conventional liquid-nitrogen boiling point in order to remove almost completely those effects (like thermal diffuse scattering and anharmonicity) that could affect (more or less severely) the overall data quality. While a general improvement is always expected, the use of very low temperatures sometimes has also revealed qualitative features otherwise unobservable (Iversen *et al.*, 1997).

Accurate electron-density mapping can be considered as a focus of an analysis starting with crystal structure determination and developing through refinement of empirical and chemical models, sometimes in connection with structural correlation methodology (Bürgi & Dunitz, 1994), which samples a given fragment in several structural contexts. In this paper, we will use temperature not only as a tool to obtain the best static density models but also as an effective variable to scan molecular conformational space, gaining more insights into the chemical bonding features than a 'traditional' experimental charge-density study. Molecules that may fit the purpose of studying the evolution of bond features upon conformational changes are organometallic complexes, where some soft metal–ligand or metal–metal interactions can be strongly affected by the intermolecular environment. We present here two multitemperature studies on salts of $[FeCo(CO)_8]^-$ (I) and $[Cr_2H(CO)_{10}]^-$ (II).

Transition-metal carbonyl dimers are widely investigated because they represent a prototype class of compound for the understanding of larger metal cluster molecules. Among the frequent theoretical or experimental works on them, many electron-density studies have appeared, see Macchi & Sironi (2003*a*) for a more comprehensive summary. The idea proposed throughout recent publications (Macchi *et al.* 1998, 1999, 2002) was to scan the conformational space of the simple homoleptic dimeric system $[M_2(CO)_n]^{m-}$, focusing on the metamorphosis of a carbonyl ligand from terminal stereochemistry (*i.e.* bound just to one metal) into that of a symmetric bridge. In other words, we adopted for charge-density studies the same criteria as used on work on the structural correlation principle, where structural (or charge-density) variations of the selected molecular fragment may inform us on the shape of its potential-energy surface. The atoms in molecules theory (Bader, 1990) was used as the tool to link the more traditional bonding concepts, based on approximated molecular-orbital theories, to the actual electron-density distributions. In that series of studies, we first detected that the bridging situation was reflecting multicentre bonding, mainly because of the absence of a metal–metal bond path and because of the inward curvature of the paths at the bridging carbonyl carbon [see scheme (III*b*) in Fig. 1]. Further analysis, based on the use of the interatomic delocalization indices δ (Bader & Stephens, 1975), showed that, even in the apparently 'pure' terminal ligands configuration [scheme (I) in Fig. 1], the system is somewhat reminiscent of a multicentre bonding, producing only a partial (typically 1/2) bond order between the two metals and some (weaker) 1,3 $M\cdots$CO interactions (see scheme in Fig. 1). Therefore, the conversion reaction path from one isomer to the other, retrievable from crystal structures deposited in the Cambridge Structural Database (CSD), could be related to the corresponding elec-

Table 1
Summary of data collection and model refinement results for $[FeCo(CO)_8][PPN]$.

$R_{int} = \sum |F_o^2 - F_{mean}^2| / \sum F_o^2$; $R_\sigma = \sum \sigma(F_o^2) / \sum F_o^2$; $R_1 = \sum ||F_o| - |F_c|| / \sum |F_o|$; i.a.m. is the conventional spherical-atom refinement of positional and thermal parameters; the ED model includes a frozen multipolar model, based on the accurate refinement of the most extensive 125 K data set; the ED+anh. model is the same as ED, plus additional variables of Gram–Charlier expansion assigned to Fe, Co, C1, O1 atoms. Refinements for which a tight convergence criterion was not met have agreement indices in italics (in particular, refinements of the 323 and 343 K data including anharmonic motion were extremely unstable).

T (K)	R_{int}	R_σ	Total reflections	Unique reflections	$(\sin\theta/\lambda)_{max}$ (Å^{-1})	V (Å^3)	R_1 (i.a.m)	R_1 ED	R_1 ED+anh.
28	0.0315	0.0394	41847	20647	0.91	1968.77	0.0370	0.0303	0.0291
125	0.0230	0.0301	102256	32676	1.07	1982.44	0.0377	0.0289	0.0288
160	0.0361	0.0577	35888	17191	0.82	1999.57	0.0440	*0.0359*	*0.0347*
200	0.0327	0.0539	25930	13687	0.77	2013.29	0.0450	0.0373	0.0351
240	0.0350	0.0594	27497	13945	0.77	2028.73	0.0491	0.0414	*0.0375*
270	0.0383	0.0635	29574	14087	0.77	2042.49	0.0522	0.0452	*0.0403*
295	0.0418	0.0659	37935	17750	0.83	2058.10	0.0565	*0.0498*	*0.0427*
323	0.0311	0.0336	15569	5938	0.56	2069.26	0.0438	*0.0379*	(*0.0322*)
343	0.0245	0.0376	11737	5911	0.56	2082.96	0.0432	*0.0396*	(*0.0349*)

tron-density rearrangement, observed experimentally in several systems and confirmed by forcing (theoretically) a single molecule (I) to reproduce the same 'experimental' path.

While performing the analysis on one salt of (I) (which has a semibridging carbonyl), we found that there was a significant difference between the gas-phase optimized geometry and the low-temperature crystal structure: in particular, the semibridging carbonyl significantly shortened its distance to Fe, elongating in turn its distance from Co. A similar discrepancy is found between the room-temperature geometry (reported by Chin *et al.*, 1974) and the low-temperature experiment. For this reason, several X-ray diffraction experiments in the 28–373 K temperature range were undertaken, showing a significant variation of the coordination of the semibridging CO ligand, owing to a soft mode associated with the Fe—C1 stretching, which can be analysed by a scan of the conformational space with theoretical investigation.

The evolution of compound (II) is also worth studying. $[Cr_2H(CO)_{10}]^-$ is a prototypical metal dimer supported by a hydride ligand and several X-ray and neutron diffraction experiments have been carried out on this species, crystallized as salts of different cations. Remarkably, the different crystalline environments result in conformational changes of the two $Cr(CO)_5$ moieties (the molecular symmetry changing, approximately, from C_s to C_{2v}). With the aim to study the accurate electron density in one of these salts, namely the $[K(crypt\text{-}222)]^+$ (crypt-222 = $C_{18}H_{36}N_2O_6$), which had been reported also from neutron diffraction by Petersen *et al.* (1981), we carried out X-ray diffraction experiments at several temperatures (in the range 28–295 K). The lowest T data collection was found to be necessary for two main reasons: (*a*) the available neutron diffraction parameters (fundamental to describe the relevant H atom) had been derived in a 20 K experiment, too far from 90 K (or above) to be safely used, even if rescaled; (*b*) the movement of the cryptate is still rather large at higher temperatures and significant changes occur to the cation–anion interaction (shortened by about 0.15 Å on passing from RT to 28 K).

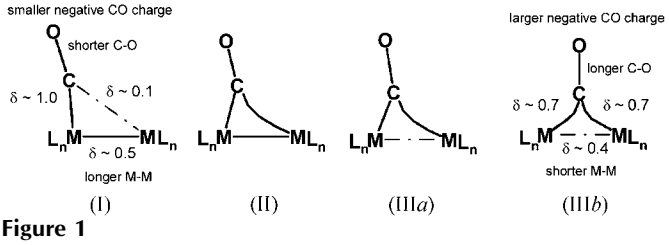

Figure 1
Scheme of the molecular graph evolutions as a function of the configurational changes of the M_2CO fragment. Solid bold lines represent schematic bond paths; dashed lines represent significant delocalization indices in the absence of a direct bond path. Note that, upon formation of a bridge, the $M—M$ density is progressively withdrawn by the more acidic carbonyl, with consequent rupture of the $M—M$ bond path. Along the conversion, the total delocalization (made by one $M—M$ and several $M—C$ electron sharing) is almost preserved. (III*a*) and (III*b*) differ only in the asymmetry of the former. In scheme (I), $\delta \sim 0.1$ occurs between all equatorial CO's bound to one side metal and the opposite metal.

2. Experimental section

The X-ray diffraction instruments installed in our laboratory and used for the experiments described below consist of a Bruker SMART CCD 1000 diffractometer, equipped with an Oxford Cryosystem liquid-N_2 cryostream (600 series), operating in the 90–373 K range, and an Oxford Cryosystem Helix, operating down to 27.5 K. Both instruments have been calibrated using a phase-transition material (Farrugia *et al.*, 2003), reproducing the results within 2 K; temperature oscillations are within 0.2 K at each point. The 90 K experiment on $[Cr_2H(CO)_{10}][K(crypt\text{-}222)]$ was instead carried out on a Bruker APEX CCD equipped with Bruker Kryoflex, while the 125 K experiment on $[FeCo(CO)_8][PPN]$ [PPN = $(Ph_3P)_2N$] was carried out on the SMART, but equipped with Bruker LT3. Typical settings of the generators are 50 kV and 30 mA for the APEX and 45 kV and 40 mA for the SMART. Mo $K\alpha$ radiation from a fine-focus sealed tube, a 0.5 mm collimator and graphite monochromator were used.[1]

[1] Supplementary data for this paper are available from the IUCr electronic archives (Reference: XC5007). Services for accessing these data are described at the back of the journal.

Table 2
Summary of data collection and model refinement results for $[Cr_2H(CO)_{10}][K(crypt\text{-}222)]$.

See caption of Table 1 for description of indices. The ED model was freely refined on 28, 90 and 113 K data sets, while it was kept frozen (to the 28 K one) for the 160 and 295 K sets. U^{ij}'s of H atoms were scaled according to an isotropic expansion.

T (K)	R_{int}	R_σ	Total reflections	Unique reflections	$(\sin\theta/\lambda)_{max}$ (Å^{-1})	V (Å^3)	R_1 (i.a.m)	R_1 ED
28	0.0391	0.0446	128749	30760	1.05	3571.87	0.0409	0.0263
90	0.0346	0.0350	179895	42694	1.15	3600.69	0.0513	0.0396
113	0.0425	0.0576	86843	29059	1.05	3618.77	0.0463	0.0335
160	0.0499	0.0413	84681	16777	0.82	3650.62	0.0421	0.0299
295	0.0453	0.0417	64936	12135	0.74	3747.71	0.0461	0.0344

Table 3
Results of rigid-body libration correction on (I) and comparison (by means of root-mean-square distances) with gas-phase geometries, optimized at the B3LYP level of theory using all electrons (a.e.) or effective core potential (e.c.p.) basis sets (the r.m.s. distance between the 28 and 343 K geometries is 0.107 Å).

The r.m.s. residual U^{ij}'s (from those of a pure rigid-body motion) and the four most relevant interatomic distances are also given. No standard uncertainty is available for these measurements; uncorrected distances have uncertainties, at worst, of 0.006 Å (for the two high-temperature structures). At all T, the i.a.m. and the ED models produce an almost identical correction, except at 323 and 343 K (reported on separate line).

T (K)	R.m.s. (Å) expt geom-B3LYP/e.c.p.	R.m.s. (Å) expt geom-B3LYP/a.e.	R.m.s. ΔU^{ij} (Å^2)	d(Fe—Co) (Å)	d(Co—C) (Å)	d(Fe—C) (Å)	d(C—O) (Å)
28	0.190	0.199	0.0007	2.619	1.836	2.156	1.181
125	0.180	0.190	0.0013	2.617	1.832	2.160	1.180
160	0.172	0.184	0.0020	2.620	1.834	2.169	1.176
200	0.170	0.182	0.0024	2.621	1.828	2.183	1.178
240	0.167	0.182	0.0029	2.621	1.823	2.206	1.177
270	0.166	0.183	0.0034	2.620	1.821	2.231	1.172
295	0.168	0.186	0.0036	2.621	1.822	2.250	1.174
323	0.170	0.190	0.0047	2.618	1.825	2.279	1.165
323-ED	0.170	0.190	0.0048	2.619	1.816	2.282	1.176
343	0.172	0.194	0.0052	2.617	1.810	2.298	1.184
343-ED	0.172	0.193	0.0052	2.627	1.802	2.292	1.195
B3LYP/a.e.				2.700	1.828	2.251	1.171
B3LYP/e.c.p.				2.667	1.807	2.298	1.176

2.1. Data collections on $[FeCo(CO)_8][PPN]$

Details of the data collection at T = 125 K and the multipolar model derived have been given in a previous publication (Macchi *et al.*, 2002). A different crystal was used for data collection at T = 160, 200, 240, 270, 323 and 343 K, where three sets of 600 frames (20 s frame^{-1}) were measured. At 28 K, four sets of frames were measured. The RT experiment, on a third crystal, consists of five sets of frames (30 s frame^{-1}), conducted in the absence of nitrogen flow. The T of this data collection can be reasonably estimated in the range 290–300 K, therefore it will be assigned a 295 K value, but it is quite evident that this experiment was the least accurate, in terms of temperature control. Data integration was performed with the *SAINT* program (Bruker–Nonius AXS, 2001) and an empirical absorption correction was applied with *SADABS* (Sheldrick, 2003). For the two highest temperatures, the integration was limited within $2\theta < 50^\circ$ due to lack of significant intensities at higher angles. Other details of each data collection are given in Table 1. Based on conclusions given below, a full data collection at the lowest T was judged unnecessary.

Differential scanning calorimetric and thermogravimetric analyses showed that above 353 K the crystals undergo a transition that produces amorphous material (in fact, diffraction is completely lost above that temperature). A weight loss then occurs at about 400 K and, eventually, the melting point is observed at about 453 K. Therefore, the relatively good quality of the data collected at 343 K is quite surprising, being so close to the rapid transformation into amorphous material.

2.2. Data collections on $[Cr_2H(CO)_{10}][K(crypt\text{-}222)]$

$[Cr_2H(CO)_{10}][K(crypt\text{-}222)]$ crystallizes in the $P2_1/c$ space group. Yellow crystals of largest dimension less than 0.3 mm were selected from several batches and tested in diffraction. A preliminary room-temperature (295 K) study was carried out on the APEX-CCD without an extensive data collection (four sets of 600 frames each, 20 s frame^{-1}), also because of the inadequate scattering power at higher diffraction angles. A complete experiment (eight sets of frames at different 2θ angles and time per frame) was then undertaken, on a second crystal, at 28 K, which is the lowest T reachable in our laboratory and sufficiently close to that used in the published

neutron experiment data (20 K) (Petersen *et al.*, 1981). Data on the same crystal were then collected at 113 K but this experiment was interrupted before reaching the desired data completeness due to a problem with the nitrogen stream apparatus. Nevertheless, this data set is quite usable. The experiment was repeated on another crystal (because of the long-period air instability of the species) at 90 K, on the APEX CCD. Finally, a 160 K data collection, on a fourth crystal, was performed on the SMART CCD.

Details of these data collections are given in Table 2.

2.3. Model refinements

Refinements against squared structure-factor amplitudes were carried out using *SHELX97* (Sheldrick, 1997), within the *WINGX* package (Farrugia, 1999), for independent-atom models (i.a.m.), and *XD* (Koritsanszky *et al.*, 2003), for the multipolar model (ED), which uses the Hansen & Coppens (1978) formalism. *XD* was also used for deriving electron-density properties and relative topology of the experimentally refined models.

For PPN salts of (I), independent-atom models were refined for each data set, using intensities above the $2\sigma(I)$ level. The best multipole model refined with the extensive data collection at 125 K was employed (frozen) at all other temperatures, allowing refinement of atomic positional and thermal parameters only, together with the scale factor. Models that include anharmonic treatment of the atomic motion for the metals and the two semibridging atoms were also refined (including anharmonicity on all atoms of the anion would exceed safe data/parameter ratios, especially for the higher-temperature models). No significant extinction effect was detected on any of the three crystals selected. All geometries were corrected for thermal libration effects (although the assumption of a rigid body is particularly weak for the higher-temperature refinements, as demonstrated by larger U^{ij} residuals printed in Table 3).

For (II), the available neutron parameters were used for all H atoms. In the 28 K model, both positions and U^{ij}'s were used as known, because of the close agreement between the X-ray and the neutron results for the heavy atoms [$\langle U^{ij}(\mathrm{N})/U^{ij}(\mathrm{X})\rangle$ = 0.98 (2) and the average absolute error on U^{ij} is below 10%]. At all other T, H-atom U^{ij}'s were scaled according to the average $U^{ij}(\mathrm{N})/U^{ij}(\mathrm{X})$ ratio of the heaviest atoms. Positions were refined only for the 295 K model, owing to the shift occurring in the rest of the molecule. At 28, 90 and 113 K, a full multipolar model was refined, including up to quadrupoles for H atoms, up to octupoles for C, O and N atoms, up to hexadecapole for Cr atoms. The K atom was kept as a spherical cation without refining a population parameter. Sets of radial scaling parameters were refined for each chemically different atom type. At 160 and 295 K, the ED model was kept equal to that of the 28 K model and positional and thermal parameters only were refined. In a further model, anharmonic thermal parameters were assigned to the metals but at all temperatures this did not result in significant improvement.

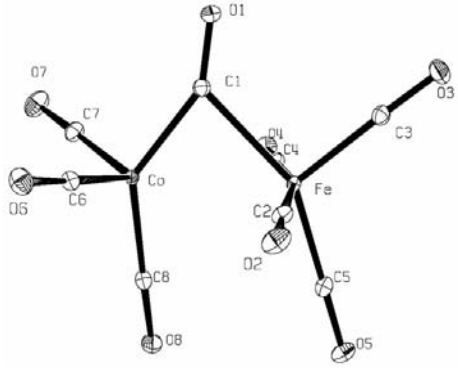

Figure 2
ORTEP view of the anion $[FeCo(CO)_8]^-$ at 28 K (ellipsoid probability at 50% level). The labelling scheme is also reported.

2.4. Theoretical calculations

Details of the theoretical calculations are reported in Macchi & Sironi (2003*a*). Here, we simply remind readers that a DFT hybrid method (B3LYP) was used for geometry optimization with two kinds of basis sets: (*a*) relativistic small-core effective core potentials (Hay & Wadt, 1985), with a basis-set splitting (341/311/41) for the metals and double-zeta-quality (Dunning & Hay, 1976) all-electron basis (721/41) for C and O atoms, with two polarization *d* functions on C and O atoms (basis set e.c.p.); (*b*) all-electron basis set of 6-311++G quality for both the second-row elements and the metals, including one polarization *d* function for second-row atoms and one *f* function for the metals (basis set a.e.). The program *AIM2000* (Biegler-König, 2002) was used to analyse the theoretical electron densities.

3. Results and discussion

3.1. The semibridging carbonyl shift in $[FeCo(CO)_8]^-$

In our original study, the $[FeCo(CO)_8]^-$ anion (Fig. 2) was selected because of its semibridging carbonyl, 'donated' by the electron-richer $Co(CO)_4$ moiety to the electron-poorer $Fe(CO)_4$ one, offering an $M-(CO)-M$ system somewhat intermediate between that of a 'purely' unsupported $M-M$ bond {of $[Co_2(CO)_6(AsPh_3)_2]$} and a symmetric bridge {of $[Co_4(CO)_{11}PPh_3]$}, both determined at the level of accurate electron density [Macchi *et al.* (1998) and (1999), respectively].

The interesting molecular rearrangement that occurs to this molecule, in its PPN salt, on varying the temperature encouraged us to study this evolution with the aim of gaining some additional information. As described in the *Introduction*, the low-temperature geometry differs from the gas-phase theoretical optimization mainly because of the shorter distance between Fe and the semibridging carbonyl. At higher temperatures, instead, the Fe—C1 distance is closer to the theoretical prediction (see Table 3). The Fe—C1 compression is 'compensated' by Co—C1 and C1—O1 elongation, in good agreement with the path retrieved from the CSD analysis.

The shift of the semibridging carbonyl is correlated to a relaxation of the $Fe(CO)_4$ moiety, which mainly involves the coplanar terminal carbonyls 3 and 5, see Fig. 3.

In Table 3, the root mean square (r.m.s.) distances between experimental (libration corrected) and theoretical geometries are tabulated [using the procedure of the routine *IDEAL* (Gould *et al.*, 1988)]. These data give some important information: (*a*) the low-temperature geometry, though more accurately determined, is the most deformed with respect to that of the isolated (C_s symmetry) molecule; (*b*) the high-temperature geometry, although closer to the gas phase because of the reduced effect of the crystalline environment, is the least accurate owing to the larger molecular motion; (*c*) as a result, the gas-phase and solid-state geometries are apparently closer in the range 200–270 K; (*d*) for all points, the all-electron basis set (a.e.) performs less satisfactorily than the effective core potential (e.c.p.). The latter observation is important because geometry optimization with e.c.p. is much less expensive, even if the reconstruction of the total electron density is then problematic.

Looking in more detail at the part of the molecule that is most interesting for our study, libration-corrected interatomic distances (Schomaker & Trueblood, 1968) show quite nicely the correlation along the temperature range investigated, with the exception of the semibridging C—O distances at 323 and 343 K, which clearly look like outliers. (Noteworthy is that, at least for the 323 K model, including frozen multipoles from the 125 K model produces more satisfactory corrected distances.) The reason why such a large phenomenon occurs has to be related to the quite soft bonding established between a metal (Fe) and the semibridging carbonyl, whose stretching frequency is estimated to be *ca* 50–70 cm^{-1}, depending on the theoretical method. One may argue that Fe—Co is also a weaker bonding (even with a vanishing direct interaction) but, as we already reported, each metal is not only interacting with the other metal but also with all its carbonyls, see Fig. 1 and Macchi & Sironi (2003*a*). Thus, a stretching along the Co—Fe direction would be much more expensive than the single Fe—C1 stretching, because it is acting not only against one *M*—*M* but also against several *M*—C attractions.

We have evaluated the crystal strain tensor ε, within the approximation of a purely harmonic crystal at 28 K, according to the formalism by Schlenker *et al.* (1978). At each temperature, the linear Lagrangian strain tensor is computed from lattice parameters, together with the total strain *Es* (square root sum of all the tensor components). The evolution of *Es* plotted in Fig. 4 (normalized to the value of 295 K) shows that only above 160 K is the strain significantly observable. The shape of the tensor is also very informative, being described by an ellipsoid oblate in the Fe—Co—C1 plane, with the principal component parallel to the Fe—C1 vector (see Fig. 3). This clearly shows that CO's soft modes are tightly connected to the crystal expansion–compression.

Es correlates very well also with the main atomic anharmonic parameters (Johnson & Levy, 1974), refined for Fe, Co, C1 and O1 in the models 28–295 K (higher *T* are omitted due to the large instability of these refinements), see Fig. 4. According to molecular changes, strain tensor and Gram–Charlier coefficients, we may conclude that anharmonic motion is not relevant at 125 K, but only above 160 K. The slight improvement for the 28 K model introduced by including anharmonic parameters seems to be related to the presence of some uncorrected absorption residuals near the two metals, which are partially fitted by the Gram–Charlier coefficients. Similar residuals are located at all temperatures but 125 K, whose data collection was more extensive (and therefore better corrected for absorption) than all the others (see Table 1). To prove that these peaks are due to incomplete data collection, we simply removed from the extensive 125 K raw data some of its subsets and saw peaks appearing close to the metals, which are absent if the full data set is used for empirical absorption correction.

Comparison of theoretical densities show that no significant electron redistribution occurs on modifying the geometry

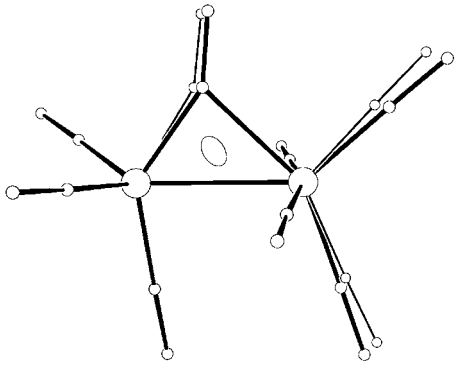

Figure 3
The shift occurring to the semibridging and three coplanar carbonyls, represented by plotting their positions in the 343 K refined structure (smaller spheres) on the 28 K overall geometry. All other smaller variations are omitted for clarity. The strain tensor, in the same framework representation, is plotted in the centre of the drawing (the out-of-plane component is small); it clearly indicates that the rearrangement occurring to the anion upon cooling–warming has a tighter connection to the actual compression–expansion of the crystal.

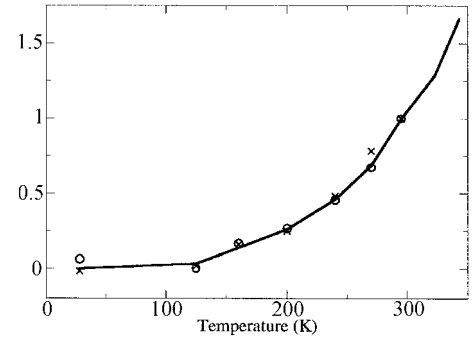

Figure 4
Evolution of the total strain (bold line) in the range 28–343 K and of the most significant anharmonic parameters (circles represent U^{2222}, averaged over Fe and Co, crosses U^{111} averaged over O1 and C1) refined in the range 28–295 K (higher temperatures are excluded due to the highly unstable refinement of these parameters which caused inconsistent results). For comparative purposes, all quantities are normalized with respect to the 295 K point.

from the high to the low temperature in the solid state. This is because the semibridging coordination mode in both cases lies in region (III) of the scheme in Fig. 1. Therefore, the metal–metal bond path is absent throughout the full molecular rearrangement. This is the reason why a frozen 125 K multipolar model can be successfully exported at all temperatures (see Table 1).

3.2. Comparison of charge-density models at two temperatures for $[Cr_2H(CO)_{10}]^-$

It is now well established that mononuclear transition-metal hydrides have a strong tendency to form di- or polynuclear assembles containing $M-H-M$ structural units and much work has been carried out to clarify their structure, reactivity, spectroscopy and bonding properties. Actually, $M-H-M$ bridging bonds are particularly interesting to study because they belong to a selected family of interactions: namely, the electron-deficient three-centre two-electron bonds, of which the B—H—B bridging bond is perhaps the best known example.

In the literature, the anion $[Cr_2H(CO)_{10}]^-$ has been studied as a salt of different cations and some experimental determinations were carried out also with neutron diffraction techniques. Therefore, we decided to start an X-ray investigation of the electron density of one of those crystalline forms whose neutron diffraction results (measured at 20 K) were known, namely $[Cr_2H(CO)_{10}][K(crypt\text{-}222)]$, shown in Fig. 5.

It is interesting to note that the molecular conformation of (II) depends on the type of environment and ranges from a pseudo C_s symmetry [with staggered carbonyl (Klufers & Wilhelm, 1991)] to a pseudo C_{2v} [with quasi-eclipsed carbonyls (Petersen *et al.*, 1978)], with consequent modification of the Cr—H—Cr angle as well, see Fig. 6. The analysis of the bonding features and their changes upon conformational rearrangement is the subject of a future work, while here we will focus on two aspects related to multitemperature measurements: (*a*) the effects of the temperature on the data-collection quality; (*b*) the effects of the temperature on geometries, which, this time, do not affect so severely the molecular conformation but rather the intermolecular coordination. After correction for thermal libration effects, the RT and the 28 K geometry have r.m.s. deviations of 0.055 Å (for the anion) and 0.031 Å for the cation, however the anion–cation coordination, which occurs through the O1—K bond (see Fig. 5), undergoes an important shortening from 3.117 (2) to 2.967 (1) Å, mainly due to a contraction of the crypt-222 ether (overall the baricentres approach from 6.39 to 6.26 Å). This effect is responsible for the overall unit-cell contraction upon cooling, but the strain tensor is scarcely informative here, being almost isotropic ($\varepsilon_{ii(\max)}/\varepsilon_{ii(\min)} < 1.5$). A slight shortening of the Cr—Cr distance is also observed, followed

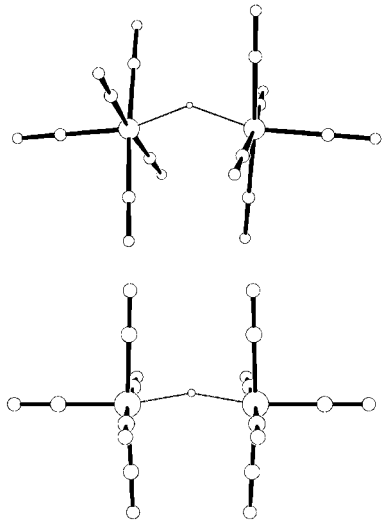

Figure 6
The two conformational limits, pseudo C_s (top) and pseudo C_{2v} (bottom) of the anion $[Cr_2H(CO)_{10}]^-$, observed in salts of $[Cu(PPh_3)_3]^+$ and PPN, respectively.

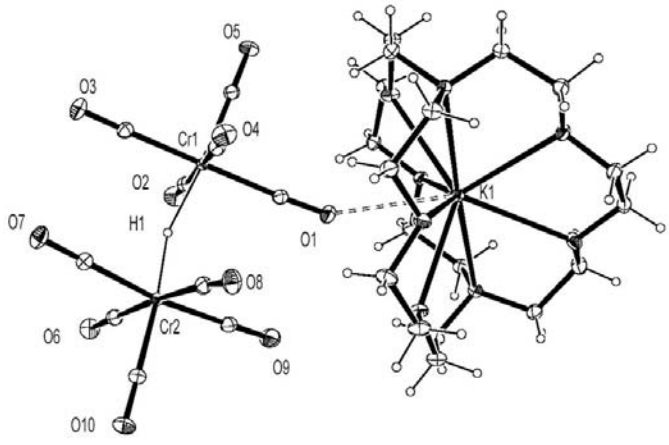

Figure 5
ORTEP view of the 28 K structure of the anion (II) and the cation K(cryp-222), which are coordinated through the O1···K1 bond. Selected labels only are reported for the sake of clarity. Ellipsoids at 70% probability level; H atoms are drawn as small spheres.

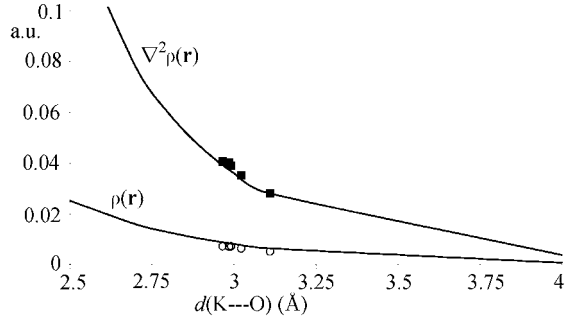

Figure 7
Evolution of topological indices (in atomic units) as a function of K—O distance (in Å), which changes with the temperature. Circles and squares are the $\rho(\mathbf{r})$ and $\nabla^2\rho(\mathbf{r})$ at critical points, derived from experimental models from 28 to 295 K (160 and 295 K are refined with fixed coefficients from the 28 K model). Solid lines represent theoretical predictions (B3LYP/a.e.) on a prototype $K[CrH(CO)_5]$ complex, with $[CrH(CO)_5]^-$ approaching in an end-on mode the K^+ (in isolation, the minimum distance is attained at 2.45 Å).

by 'rigid' movements of the two $Cr(CO)_5$ units, especially above 113 K.

The translation of the anion and the cation on lowering the temperature is associated with the contraction of the K(1)—O(1) distance and with a consequent increase of the electron density at the relative bond critical point. This is outlined in Fig. 7, where the experimental trend is compared with the theoretical one, simulated by a mutual end-on approaching of K^+ to $[OC–Cr(CO)_4H]^-$.

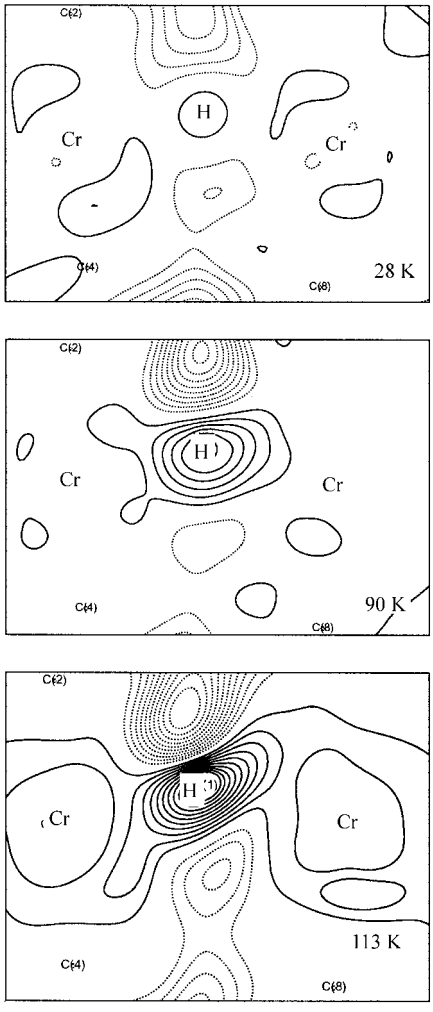

Figure 8
Relative $\Delta\rho(\mathbf{r})$ difference density maps between experimental and theoretical (B3LYP/a.e.) densities in (II). From top to bottom: 28, 90 and 113 K geometries are shown. $\Delta\rho(\mathbf{r})$ are normalized to the theoretical $\rho(\mathbf{r})$, so that each contour here represents a 10% difference (solid lines positive, dotted negative), rather than an absolute value. In this way, features at nuclear positions, due mainly to the use of Gaussian-type (theor.) instead of Slater-type (exp.) orbitals, are removed and possible smaller features in the bonding regions are enhanced. The significant features 'outside' the molecular region arise from the different treatments of the diffuse density in the theoretical (isolated) and in the experimental (extracted from crystal) molecules. Here, the 28 K map is sufficiently flat inside the three-centre bonding region, while the description at the H-atom site is problematic at higher temperatures (where neutron parameters are not available). At 113 K, the error is somewhat propagated also to the metals.

For the analysis of Cr—H—Cr three-centre bonding, the thermal parameters of the hydridic H atom, obtained through neutron diffraction, are fundamental in order to describe best the deformation density coefficients. In particular, bonding properties strongly depend on the atomic quadrupoles that affect the shape of Cr—H bond paths and the nuclear quadrupole coupling tensor. Therefore, at temperatures far from that of the neutron experiment (where a scaling of U^{ij}'s is necessary), some unexplained residuals might localize on the hydride due to a non-linear behaviour of vibration tensor components and to its positional shift (though small) due to a translation of the whole anion from the lowest-T position. As a matter of fact, the models derived from extensive data collections at 90 and 113 K differ from the 28 K model mainly in the region of the hydride bridge (at least as concerns the anion molecule). This is also evident from comparison with theoretical density, see Fig. 8.

The bonding features of the Cr—H—Cr system will be discussed elsewhere (Macchi, Donghi & Sironi, 2004) and here they are simply resumed. Owing to the long Cr—Cr distance and large Cr—H—Cr angle, a direct metal–metal bond path is absent and the Cr—Cr delocalization is very small. The central H atom has 'quadrupolar' elongation almost parallel to the Cr—Cr direction, preventing the formation of inward curvature of the bond paths, thus quite at variance with carbonyl bridges. Theoretical investigations of the gas phase suggest that a flat potential-energy surface is associated with (II) [see Richardson *et al.* (2001); further discussion in Macchi, Donghi & Sironi (2004)] and, despite the fact that the geometry may change quite importantly, the topological parameters do not vary so significantly.

4. Concluding remarks

Electron-density studies at different temperatures are usually adopted to test the reliability of a refined model in different experimental conditions. However, significant information to complement the bonding characterization is actually contained in such experiments, even on the internal vibration modes (Bürgi & Capelli, 2000; Bürgi *et al.*, 2000). In addition, temperature-dependent phenomena may sometimes bring a 'different' molecule under our microscope: for example, spin transition, electron trapping (Wilson *et al.*, 2000) and 'crystal compression' of soft bonds. In the luckiest event, any system is suitable for charge-density analysis, however the thermal energy required to see conformational changes may hamper an accurate X-ray diffraction experiment. For example, in $[FeCo(CO)_8][PPN]$, significant molecular reorganization is observed only above 160 K and thus in a range where 'accurate electron-density mapping' of a molecular crystal is itself an oxymoron. The same would be true for strong intermolecular bonds, such as hydrogen bonds in the covalent regime. Therefore, the information from molecular distortions upon varying the temperature on a given solid can, in general, be used 'only' as a complement to the bonding investigation though with enormous information on the assessment of the best theoretical model.

The safer way to obtain significant bonding information on a 'distorted' system is to induce the molecular rearrangement by changing 'chemically' the crystalline environment, a work that we have started (Macchi & Sironi, 2003*b*; Macchi, Garlaschelli & Sironi, 2004) on a series of metal cluster anions crystallized with several different cations.

On the other hand, soft modes affecting weaker intermolecular bonds, such as the one observed in $[Cr_2H(CO)_{10}][K(crypt\text{-}222)]$, are within the limit of suitability and could provide significant information on the initial step of a bond formation [somewhat in analogy with the atoms forming bonds suggested by Bader & Hernandez-Trujillo (2000)]. The analysis presented here could be safely extended to other systems, such as push–pull organic complexes, weaker hydrogen bonds, halogen bonds *etc.*

Of course, it is not possible to make any kind of generalization in view of the results presented in this work, as in other studies significant anharmonic contributions were found even at lower temperatures. The atomic thermal motion depends both on the strength of the internal bond and on the above molecular packing, therefore another semibridging carbonyl might behave very differently from (I) because of the different metal–ligand back donation and the different molecule–molecule interactions in the solid state [see, however, $Fe_3(CO)_{12}$ (Farrugia, 1997)].

The authors thank Professor L. Garlaschelli and Dr D. Donghi for providing suitable crystals for the X-ray studies.

References

Bader, R. F. W. (1990). *Atoms in Molecules. A Quantum Theory*. New York: Oxford University Press.

Bader, R. F. W. & Hernandez-Trujillo, J. (2000). *J. Phys. Chem. A*, **104**, 1779–1794.

Bader, R. F. W. & Stephens, M. E. (1975). *J. Am. Chem. Soc.* **97**, 7391–7399.

Biegler-König, F. W. (2002). *AIM2000*, version 2.0, University of Applied Sciences, Bielefeld, Germany.

Bruker–Nonius AXS (2001). *SAINT. SAX Area-Detector Integration.* Bruker AXS Inc., Madison, Wisconsin, USA.

Bürgi, H. B. & Capelli, S. C. (2000). *Acta Cryst.* A**56**, 403–412.

Bürgi, H. B., Capelli, S. C. & Birkedal, H. (2000). *Acta Cryst.* A**56**, 425–435.

Bürgi, H. B. & Dunitz, J. D. (1994). *Structure Correlation*. Weinheim: VCH.

Chin, H. B., Smith, M. B., Wilson, R. D. & Bau, R. (1974). *J. Am. Chem. Soc.* **96**, 5285–5287.

Dunning, T. H. & Hay, P. J. (1976). *Modern Theoretical Chemistry*, edited by H. F. Schaefer III, Vol. 3, p. 1. New York: Plenum Press.

Farrugia, L. J. (1997). *Dalton Trans.* pp. 1783–1792.

Farrugia, L. J. (1999). *J. Appl. Cryst.* **32**, 837–838.

Farrugia, L. J., Macchi, P. & Sironi, A. (2003). *J. Appl. Cryst.* **36**, 141–145.

Gould, R. O., Moulden, N. & Taylor, P. (1988). *IDEAL*. University of Edinburgh, Scotland.

Hansen, N. K. & Coppens, P. (1978). *Acta Cryst.* A**34**, 909–921.

Hay, P. J. & Wadt, W. R. (1985). *J. Chem. Phys.* **82**, 299.

Iversen, B. B., Larsen, F. K., Figgis, B. N. & Reynolds, P. A. (1997). *J. Chem. Soc. Dalton Trans.* pp. 2227–2240.

Johnson, C. K. & Levy, H. A. (1974). *International Tables for X-ray Crystallography*, Vol. IV, pp. 311–336. Birmingham: Kynoch Press.

Klufers, P. & Wilhelm, U. (1991). *J. Organomet. Chem.* **421**, 39–54.

Koritsanszky, T., Howard, S. T., Richter, T., Macchi, P., Volkov, A., Gatti, C., Mallinson, P. R., Farrugia, L. J., Su, Z. & Hansen, N. K. (2003). *XD, a Computer Program Package for Multipole Refinement and Topological Analysis of Charge Densities from Diffraction Data*. Free University of Berlin, Germany.

Larsen, F. K. (1995). *Acta Cryst.* B**51**, 468–482.

Macchi, P., Donghi, D. & Sironi, A. (2004). In preparation.

Macchi, P., Garlaschelli, L., Martinengo, S. & Sironi, A. (1999). *J. Am. Chem. Soc.* **121**, 10428–10429.

Macchi, P., Garlaschelli, L. & Sironi, A. (2002). *J. Am. Chem. Soc.* **124**, 14173–14184.

Macchi, P., Garlaschelli, L. & Sironi, A. (2004). In preparation.

Macchi, P., Proserpio, D. M. & Sironi, A. (1998). *J. Am. Chem. Soc.* **120**, 1447–1455.

Macchi, P. & Sironi, A. (2003*a*). *Coord. Chem. Rev.* **238–239**, 383–412.

Macchi, P. & Sironi, A. (2003*b*). Sagamore XIV Meeting, Broome, Western Australia.

Petersen, J. L., Brown, R. K. & Williams, J. M. (1981). *Inorg. Chem.* **20**, 158–165.

Petersen, J. L., Johnson, P. L., O'Connor, J., Dahl, L. F. & Williams, J. M. (1978). *Inorg. Chem.* **17**, 3460–3469.

Richardson, N. A., Xie, Y., King, R. B. & Schaefer, H. F. (2001). *J. Phys. Chem. A*, **105**, 11134–11143.

Schlenker, J. L., Gibbs, G. V. & Boisen, M. B. Jr (1978). *Acta Cryst.* A**34**, 52–54.

Schomaker, V. & Trueblood, K. N. (1968). *Acta Cryst.* B**24**, 63–76.

Sheldrick, G. M. (1997). *SHELX97. Program for the Refinement of Crystal Structures.* University of Göttingen, Germany.

Sheldrick, G. M. (2003). *SADABS v2.10*. University of Göttingen, Germany.

Wilson, C., Iversen, B. B., Overgaard, J., Larsen, F. K., Wu, G., Palii, S. P., Timco, G. A. & Gerbeleu, N. V. (2000). *J. Am. Chem. Soc.* **122**, 11370–11379.